

Stress distribution characteristics in dental implant influenced by its wall thickness

R.C. van Staden, H. Guan & Y.C. Loo

Griffith School of Engineering, Griffith University, Gold Coast Campus, Queensland 4222, Australia

N.W. Johnson

School of Dentistry and Oral Health, Griffith University, Gold Coast Campus, Queensland 4222, Australia

N. Meredith

Neoss Pty Ltd, Harrogate HG1 2PW, United Kingdom

ABSTRACT: This paper aims to evaluate the stress characteristics within the dental implant influenced by different implant wall thicknesses as a result of varying diameters of 3.5 and 5.5mm. A two-dimensional finite element model of the implant and mandibular bone consisting of triangular and quadrilateral plane strain elements is analysed to compute the von Mises stresses in the implant subjected to varied masticatory forces and abutment screw preloads. As expected the implant wall thickness significantly influences the stress magnitude and distribution pattern within the implant. Stress concentrations generally occur at the top of the implant as well as around the notch. When the wall thickness is reduced, stress concentrations are also found around the first external implant thread. The results also show that the masticatory force is more influential on the stress within the implant than the abutment screw preload.

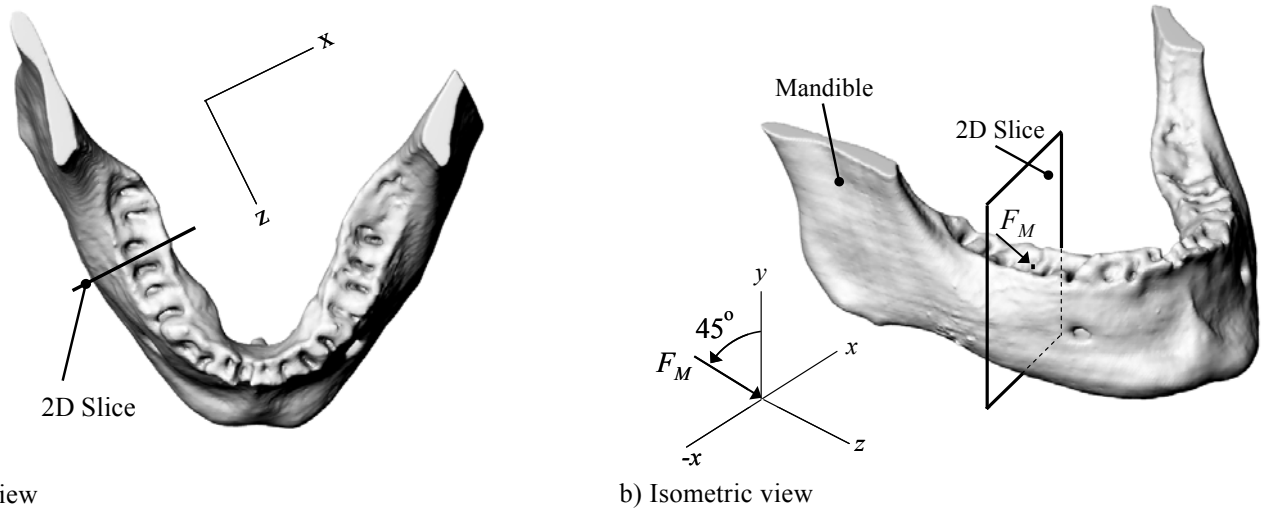
1 INTRODUCTION

The modern dental implant is a biocompatible titanium device surgically placed into the jawbone to support a prosthetic tooth crown in order to replace missing teeth. The establishment of a strong biomechanical bond between implant and jawbone is called osseointegration (Branemark et al. 1969, 1977). The success or failure of osseointegration depends on many factors including mainly: medical status of the patient, smoking habits, bone quality, bacterial contamination, immediate loading and implant surface characteristics (Esposito et al. 1998). For both early and late implant failures, loading is considered an important factor (Geng et al. 2001).

The stress characteristics within the implant are influenced by the implant dimensions, as documented by Huang et al. (2005), Capodiferro et al. (2006) and Tolman and Laney (1992). Catastrophic mechanical failure of the implant may occur by implant fatigue (Huang et al. 2005, Capodiferro et al. 2006), implant fractures, veneering resin/ceramic fractures or other mechanical reten-

tion failures (Winklere et al. 2003, Naert et al. 1992, Tolman and Laney 1992). From an engineering perspective, an important criterion in designing an implant is to have a geometry that can minimize mechanical failure caused by an extensive range of loading. van Staden et al. (2007) have shown that with reduced implant diameters the risk of failure is increased.

As part of the implantation process, the torque is applied to the abutment screw causing an equivalent preload or clamping force between the abutment and implant. This is to ensure that the various implant components are perfectly attached to each other. However, to date no published research appears to have investigated the influence of both masticatory forces and abutment screw preloading on stresses in implants influenced by the implant wall thickness due to various implant diameters. Therefore, the aim of this study is to evaluate the stresses within an immediately loaded implant under a range of masticatory forces, abutment preloads and implant diameters.



a) Top view
Figure 1. Location of 2D slice in a mandible.

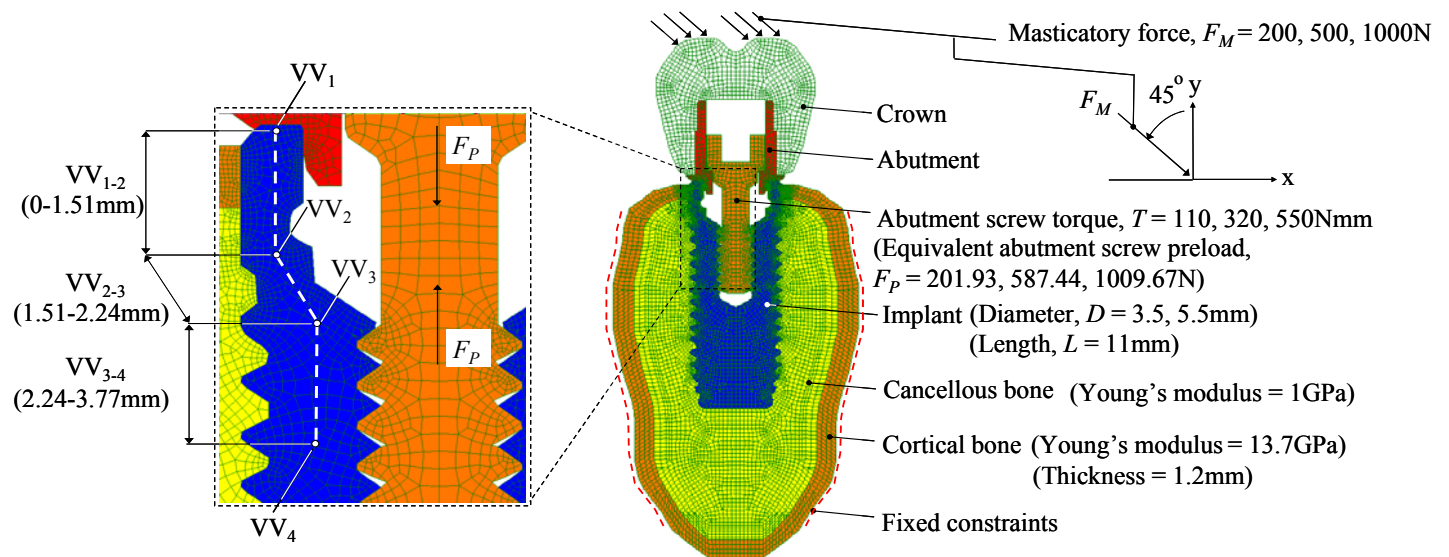


Figure 2. Finite element model of implant, components, implant/bone interface and bone.

2 METHODOLOGY

2.1 Modelling

A cross-sectional slice is taken from the mandible as shown in Figure 1. The “arc length” of the mandible is comparable to the width and depth of the slice. When the slice is subjected to in plane (x-y) masticatory forces (F_M), it is restraint from deforming out-of-plane (in the z-axis). Therefore, it can be assumed that all the strains are confined in the z-axis. To accurately represent the mechanical behavior of the implant and bone, 3-node triangular (Tri3) and 4-node quadrilateral (Quad4) plane strain elements are therefore used for the construction of the finite element models of the implant/bone system. This is presented in Figure 2.

The two-dimensional (2D) model is analysed using Strand7 (2004) Finite Element Analysis (FEA) system. Data is acquired for the bone dimensions by computed tomography (CT) scanning. Two different types of bone, cancellous and cortical, are distinguished and the boundaries are identified in order to assign different material properties within the finite element model.

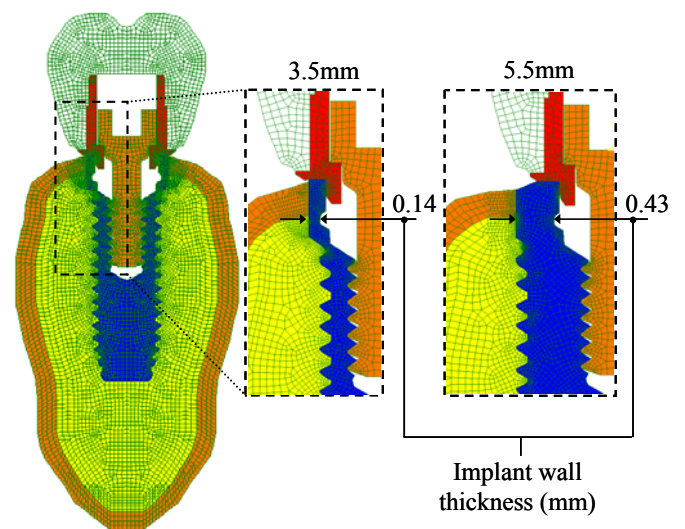


Figure 3. Finite element model showing different implant diameters.

The implant is based on that manufactured by Neoss (2006), which is conical with 2 degrees of taper and has a helical thread. Two different implant diameters (3.5 and 5.5mm) as well as the corresponding wall thicknesses are shown in Figure 3. Note that 4.0 and 4.5mm diameter implants are also popularly used and

detailed studies on all four diameters can be found elsewhere (van Staden et al. 2007).

The material properties adopted are specified in terms of Young's modulus, Poisson's ratio and density for the implant and all associated components (Table 1). All materials are assumed to exhibit linear, homogeneous elastic behavior. For the finite element model with $D = 3.5\text{mm}$, $L = 11\text{mm}$, $T_{cor} = 1.2\text{mm}$, 3314 plate elements and 3665 nodal points are used for the implant, 3804 elements and 4079 nodes for cancellous bone, and 1216 elements and 1453 nodes for cortical bone.

Table 1. Material properties

Component	Young's modulus, E (GPa)	Poisson's ratio, ν	Density, ρ (g/cm ³)
Implant, abutment, washer	105.00	0.37	4.51
Abutment screw	93.00	0.30	16.30
Crown	172.00	0.33	6.05
Cancellous bone	1.00	0.30	0.74
Cortical bone	13.70	0.30	2.19

The loading and restraint conditions as well as the detailed parameters are also illustrated in Figure 2. To evaluate the effect on stress characteristics in the implant due to varying wall thicknesses, three different mastication forces (F_M) and three different abutment preloads (F_P) are considered. The techniques for applying F_M to the crown and F_P to the abutment screw are discussed respectively in Sections 2.2 and 2.3. Note that the outer surface of the jawbone is restrained in the x, y and z directions. Note also that complete osseointegration at the implant/bone interface is assumed.

As indicated in Figure 2 the von Mises stresses along the lines VV_{1-2} (0-1.51mm in length), VV_{2-3} (1.51-2.24mm) and VV_{3-4} (2.24-3.77mm) are measured for all possible combinations of loading and diameters. These lines are approximately centre lines of the implant wall. Each line is identified by its start and end points, for example, line VV_{1-2} begins at VV_1 and ends at VV_2 . These locations were suggested by clinicians to be prone to micro fractures.

2.2 Masticatory force, F_M

During masticatory function the occlusal surface of the crown is subjected to oblique loads applied at 45° inclination in the x-y plane (refer to Figure 2). The present study assumes that the masticatory force, F_M , is set at 200, 500 and 1000N, as shown in Figure 2. The theoretical study by Choi et al. (2005) suggests that this loading condition can be considered to represent realistic loading functions.

2.3 Preload, F_P

The torque applied to the abutment screw causes the preload or the clamping force between the implant and abutment. The procedure for calculating F_P (or torque) and applying the equivalent temperature sensitive elements throughout the abutment screw is described below.

An implant system typically consists of an implant, crown, abutment and abutment screw. The method for assembly of implants involves surgically placing (or screwing) the implant into the bone. Subsequently the abutment is attached by an abutment screw, which is mechanically screwed into the internal thread of the implant using a manual screwdriver. Finally, the crown is placed on to the abutment using cement at the crown and abutment interface.

Neoss (2006) recommends that the abutment screw is tightened by a torque of 200Nmm. Note that in this study three levels of torque are considered to cover the situation of under (i.e. 110Nmm), average (i.e. 320Nmm), and over tightening (i.e. 550Nmm). The equivalent preload F_P , as a result of the torque, can be calculated through the procedure outlined below.

The nature of the forces clamping implant components together, and how they are generated and sustained, are not comprehensively covered in the literature. Preload was considered in the finite element model by Haack et al. (1995), Lang et al. (2003) and Byrne et al. (2006). These studies were based on complicated three-dimensional (3D) modeling and the techniques used for replicating F_P were inadequately specified.

The relationship between the torque applied to the abutment screw, T and the equivalent preload, F_P was suggested by Dekker (1995) as:

$$T = F_P \left(\frac{i}{2\pi} + \frac{\mu_t r_t}{\cos \beta} + \mu_n r_n \right) \quad (1)$$

where

T = torque applied to the abutment screw (Nmm)
= 320Nmm (Neoss 2006);

F_P = preload created in the abutment screw (N)
(to be determined);

i = pitch of the abutment screw threads (mm)
= 0.40mm (Neoss 2006);

μ_t = coefficient of friction between abutment screw
and internal implant screw thread surfaces
(dimensionless)
= 0.26 (Lang et al. 2003);

r_t = effective contact radius between the inner
implant and the abutment screw threads (mm)
= $(r_3 + r_4) / 2 = (0.99 + 0.755) / 2$
= 0.87mm (Neoss 2006) (see Figure 4);

β = half-angle of the threads (degree)

$$\begin{aligned}
&= 28.72^\circ \text{ (Neoss 2006);} \\
\mu_n &= \text{coefficient of friction between the face of the} \\
&\quad \text{abutment screw and the upper surface of the} \\
&\quad \text{abutment (dimensionless)} \\
&= 0.20 \text{ (Lang et al. 2003); and} \\
r_n &= \text{effective radius of contact between the} \\
&\quad \text{abutment and implant surface (mm)} \\
&= (r_1 + r_2) / 2 = (1.275 + 0.95) / 2 \\
&= 1.11 \text{ mm (Neoss 2006) (see Figure 4).}
\end{aligned}$$

Note that the effective radii (r_t and r_n) are the distances between the geometric centre of the part (implant, abutment or abutment screw) and the circle of points through which the resultant contact forces between mating parts (implant, abutment or abutment screw) pass (refer to Figure 4). Equation 1 then yields $F_P = 587.44\text{N}$.

The preload clamping the abutment to the implant is transferred through two interfaces. The first interface (SA_1) is between the abutment and abutment screw and the second (SA_2), between the abutment screw threads and inner threads of the implant (refer to Figure 4). The calculated preload, F_P , is assumed to act equally, as a pressure, q , across the first and second interfaces. Due to equilibrium, only the pressure q , acting on SA_1 is con-

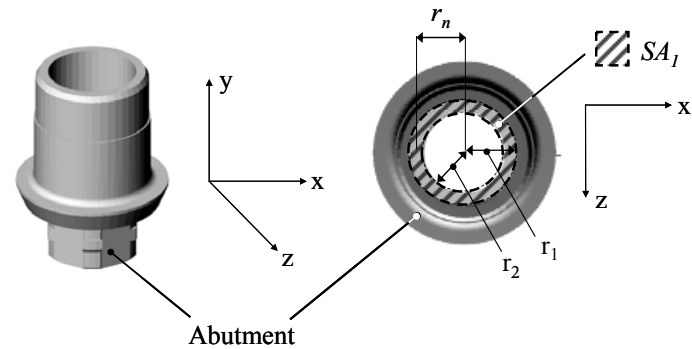
sidered in this study.

$$\begin{aligned}
SA_1 &= (\pi \times r_1^2) - (\pi \times r_2^2) = (\pi \times 1.275^2) - (\pi \times 0.95^2) \\
&= 2.27 \text{ mm}^2
\end{aligned}$$

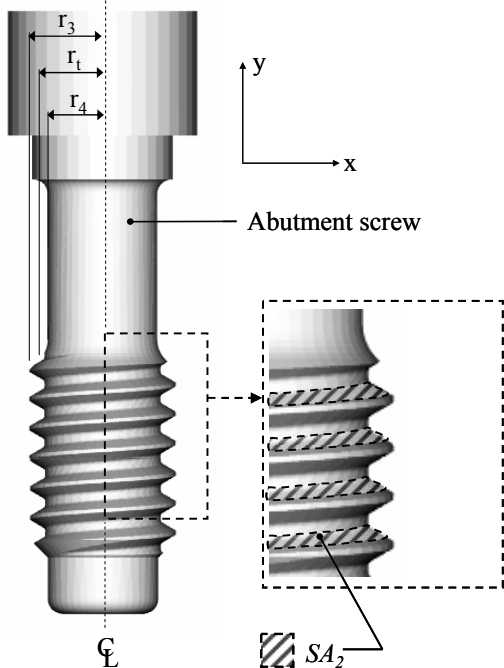
The pressure acting on SA_1 , when $F_P = 587.44\text{N}$, is calculated as follows:

$$q = \frac{F_P}{SA_1} = \frac{587.44}{2.27} = 258.22 \text{ N/mm}^2 \quad (2)$$

The clamping pressure, q , is a result of the applied torque and is a means of replicating the 3D torque in a 2D manner. For the present study, q is calculated as above for the applied torques of 110, 320 and 550Nmm (Table 2). To produce equivalent q or F_P , temperature sensitive elements are used throughout the entire abutment screw. A negative temperature (-10 Kelvin, K) is applied to all the nodal points within the abutment screw, causing each element to shrink. A temperature coefficient, C is also required in the analysis and a trial and error process is used to determine equivalent C s for different levels of F_P . In order to replicate F_P realistically, element shrinkage is allowed to occur in the y-direction only. Hence, C is applied in the y-direction as well. A summary of T , F_P , q and C is presented in Table 2.



a) Abutment



b) Abutment screw

Figure 4. Effective radii of abutment and abutment screw.

Table 2. Summary of loading.

T (Nmm)	F_P (N)	q (N/mm ²)	$C_{3.5\text{mm}}$ ($\times 10^{-12}$)	$C_{5.5\text{mm}}$ ($\times 10^{-12}$)
110	201.93	88.76	-2.62	-4.14
320	587.44	258.22	-7.61	-12.71
550	1009.67	443.83	-13.08	-20.78

3 RESULTS

The von Mises stress distributions in the implant wall are evaluated for all combinations of masticatory and preload forces and for two implant systems with different wall thicknesses.

3.1 Masticatory force, F_M

The distributions of von Mises stresses on the lines VV_{1-2} , VV_{2-3} and VV_{3-4} for all values of F_M are shown in Figure 5. Note that the preload, F_P , is set at its medium value, i.e. 587.44N. Note also that the stress profile and contour for diameter 3.5mm are shown in Figures 5a and b respectively, and those for 5.5mm are presented in Figures 5c and d respectively.

In general, when the applied masticatory force, F_M , is increased, the von Mises stresses also increase proportionally, because the system being analysed is linear elastic. As expected the 3.5mm implant shows higher stresses than the 5.5mm counterpart (refer to Figures 5a and c). The stress peaks shown in these

two figures correspond to the stress concentration areas (i.e. VV_{1-2} and VV_{2-3} for 3.5mm and VV_{1-2} for 5.5mm) as illustrated in Figures 5b and d respectively. When the wall thickness is reduced as in the case of the 3.5mm implant, the stress concentration extends from the top of the implant to the first external implant thread.

van Staden et al. (2007) found that the 4.0 and 4.5mm diameter implants have similar stress distribution characteristics, but lower stress magnitudes at VV_{1-2} , VV_{2-3} and VV_{3-4} when compared to the 3.5mm implant. The 5.5mm implant yields greatly reduced stresses at all locations with stress concentration occurring close to the top of implant only.

3.2 Preload, F_P

To investigate the effect of different preloads F_P , F_M is kept as a constant at its medium value, i.e. 500N. The distributions of von Mises stresses on the lines VV_{1-2} , VV_{2-3} and VV_{3-4} for all values of F_P are shown in Figures 6a and c for 3.5 and 5.5mm implants, respectively. The corresponding stress contours are presented in Figures 6b and d. Similar stress distribution characteristics are found when varying F_P as with F_M . Note that when F_P increases, the von Mises stresses also increase. However, the increase is not proportional to the increase of F_P . This is because F_P , as an internal force, is a function of the abutment screw and implant diameters. The large stress variations due to different F_M (Figures 5a and c) and the relatively small stress variations due to different F_P (Figures 6a and c) demonstrate that F_M is more influential than F_P to the implant system. This suggests that failure of the crown is more likely to be caused by F_M .

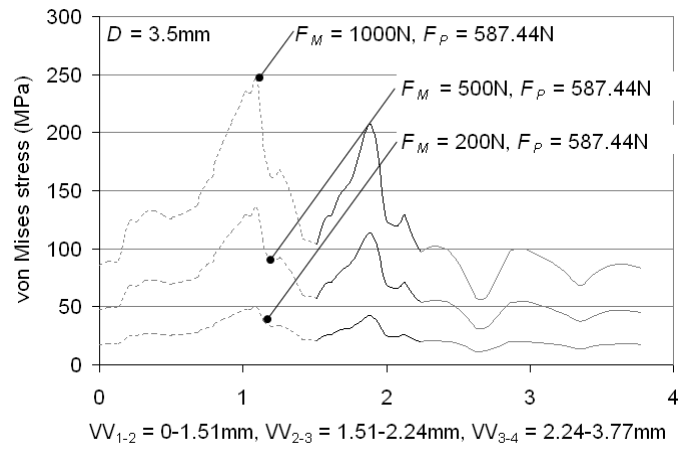
4 CONCLUSION

This study demonstrates that the implant wall thickness significantly influences the stress magnitude and distribution pattern within the implant. Stress concentrations generally occur at the top of the implant as well as around the notch. When the wall thickness is reduced, stress concentrations are also found around the first external implant thread. Overall, it is found that the masticatory force is more influential on implant stresses than the abutment screw preload.

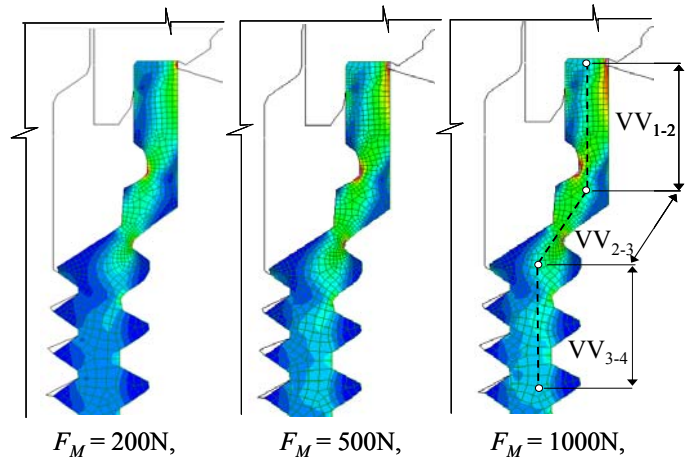
The study can be further extended to evaluate the impact of the wall thickness in other implant systems.

5 ACKNOWLEDGEMENTS

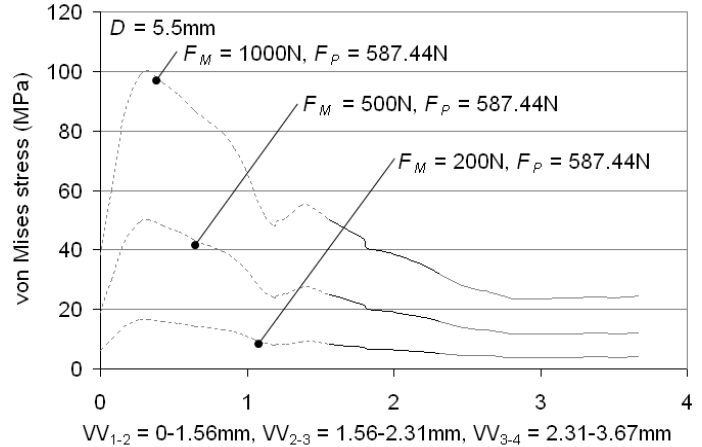
A special thank you goes to Messer John Divitini and Fredrik Engman from Neoss Limited for their continual contribution.



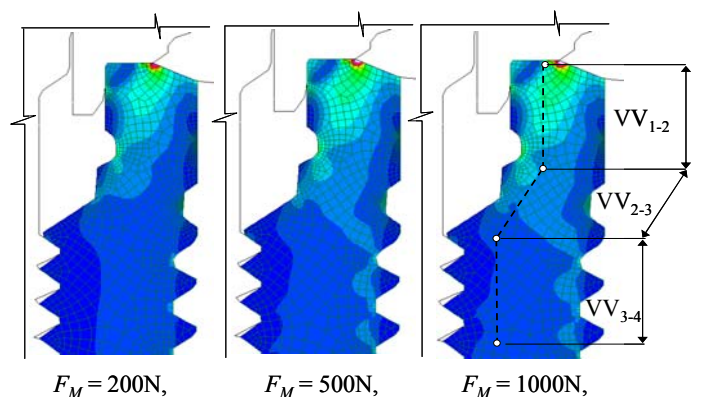
a) Stress profile



b) Stress contour

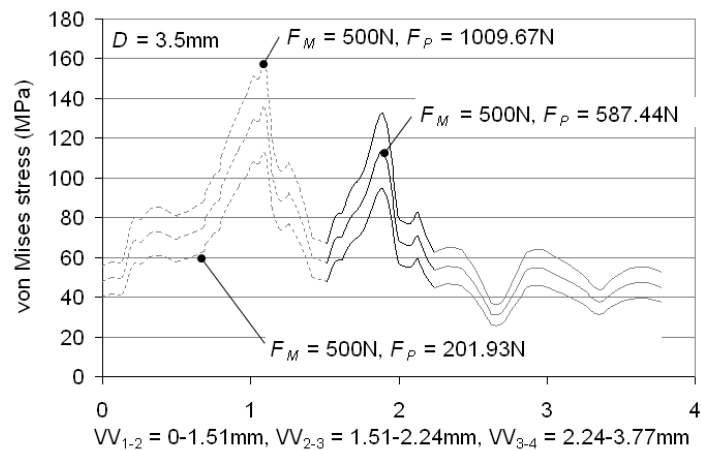


c) Stress profile

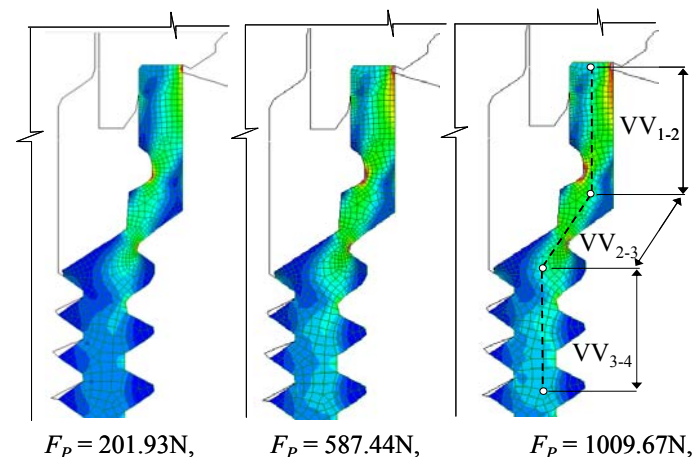


d) Stress contour

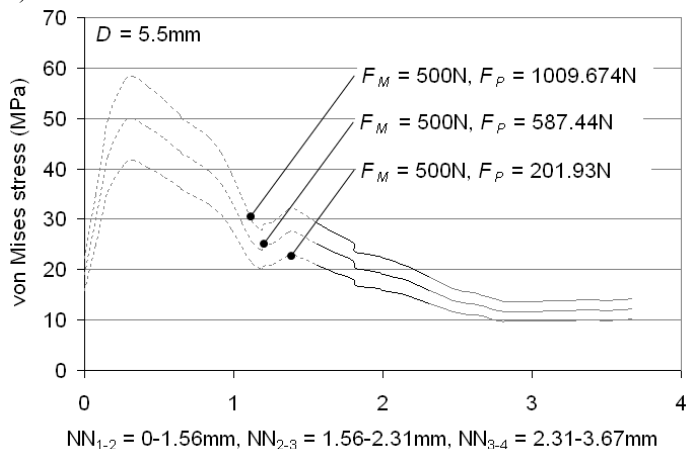
Figure 5. Stress characteristics when varying F_M .



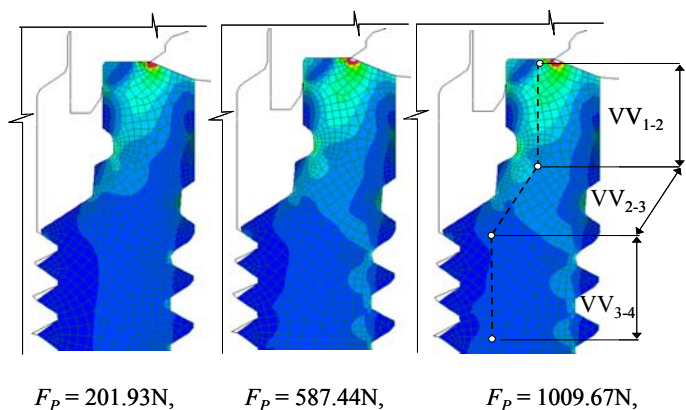
a) Stress profile



b) Stress contour



c) Stress profile



d) Stress contour

Figure 6. Stress characteristics when varying F_p .

REFERENCES

- Branemark, P.I., Adell, R., Breine, U., Hansson, B.O., Lindstrom, J. & Ohlsson, A. 1969. Intra-osseous anchorage of dental prostheses. I. Experimental studies. *Scandinavian Journal of Plastic and Reconstructive Surgery* 3(2): 81-100.
- Branemark, P.I., Hansson, B.O., Adell, R., Breine, U., Lindstrom, J., Hallen, O. & Ohman, A. 1977. Osseointegrated implants in the treatment of the edentulous jaw. Experience from a 10-year period. *Scandinavian Journal of Plastic and Reconstructive Surgery* 16: 1-132.
- Byrne, D., Jacobs, S., O'Connell, B., Houston, F. & Claffey, N. 2006. Preloads generated with repeated tightening in three types of screws used in dental implant assemblies. *The Journal of Prosthetic Dentistry* 15(3): 164-171.
- Capodiferro, S., Favia, G., Scivetti, M., De Frenza, G. & Grassi, R. 2006. Clinical management and microscopic characterisation of fatigue-induced failure of a dental implant. Case report. *Head & Face Medicine* 22(2): 18.
- Choi, A.H., Ben-Nissan, B. & Conway, R.C. 2005. Three-dimensional modelling and finite element analysis of the human mandible during clenching. *Australian Dental Journal* 50(1): 42-48.
- Dekker, M. 1995. An introduction to the design and behavior of bolted joints / John H. Bickford (3rd ed).
- DeTolla, D.H., Andreana, S., Patra, A., Buhite, R. & Comella, B. 2000. Role of the finite element model in dental implants. *Journal of Oral Implantology* 26(2): 77-81.
- Esposito, M., Hirsch, J.M., Lekholm, U. & Thomsen, P. 1998. Biological factors contributing to failures of osseointegrated oral implants. (II). Etiopathogenesis. *European Journal of Oral Sciences* 106(3): 721-764.
- Geng, J.P., Tan, K.B. & Liu, G.R. 2001. Application of finite element analysis in implant dentistry: a review of the literature. *Journal of Prosthetic Dentistry* 85: 585-598.
- Haack, J.E., Sakaguchi, R.L., Sun, T. & Coffey, J.P. 1995. Elongation and preload stress in dental implant abutment screws. *International Journal of Oral & Maxillofacial Implants* 10(5): 529-536.
- Huang, H.M., Tsai, C.M., Chang, C.C., Lin, C.T. & Lee, S.Y. 2005. Evaluation of loading conditions on fatigue-failed implants by fracture surface analysis. *International Journal of Oral & Maxillofacial Implants* 20(6): 854-859.
- Lang, L.A., Kang, B., Wang, R.F. & Lang, B.R. 2003. Finite element analysis to determine implant preload. *The Journal of Prosthetic Dentistry* 90(6): 539-546.
- Naert, I., Quirynen, M., van Steenberghe, D. & Darius, P. 1992. A study of 589 consecutive implants supporting complete fixture prostheses. Part II: prosthetic aspects. *Journal of Prosthetic Dentistry* 68: 949-956.
- Neoss Limited. 2006. *Neoss Implant System Surgical Guidelines*, UK.
- Strand7 Pty Ltd. 2004. *Strand7 Theoretical Manual*, Sydney, Australia.
- Tolman, D.E. & Laney, W.R. 1992. Tissue integrated prosthesis complications. *International Journal of Oral & Maxillofacial Implants* 7: 477-484.
- van Staden, R.C., Guan, H., Loo, Y.C., Johnson, N.W. & Meredith, N. 2007. Stress Evaluation of Implant Wall Thickness using Numerical Techniques. *Applied Osseointegration Research* (in press).
- Winkler, S., Ring, K., Ring, J.D. & Boberick, K.G. 2003. Implant screw mechanics and the settling effect: overview. *Journal of Oral Implantology* 29(5): 242-245.